Numerical simulation of side-heated free convection loop placed in transverse magnetic field; the induced electric current

Received March 1997
Revised March 1998
Accepted June 1998

Nesreen K. Ghaddar
American University of Beirut, Faculty of Engineering and Architecture, Beirut, Lebanon

Nomenclature

B_o = magnetic field strength
C_p = specific heat
D = channel width
d = half-channel width, D/2
g = gravitational acceleration
Gr = Grashof number, $g\beta\Delta TD^3/\nu^2$
h = heat transfer coefficient in the loop channel
Ha = Hartmann number, $B_oD(\sigma/\rho_o\ \nu)^{1/2}$
j = induced electric current
k = thermal conductivity of the fluid
L = vertical height of half the loop
2*l* = height of the insulated region
Nu = Nusselt number, hD/k
p = pressure
Pr = Prandtl Number, ν/α
QL = heat transfer rate carried by the loop
Ra = Rayleigh number, RePr
Re = Reynolds number, V_oD/ν
t = time
T = temperature
V_o = 1-D bulk induced velocity in the loop
U = dimensionless velocity component in x-direction, u d/α
V = dimensionless velocity component in y-direction, v d/α
(x, y, z) = Cartesian coordinates

Greek

α = thermal diffusivity
ß = thermal expansion coefficient
ΔT = temperature difference between hot and cold segments, T_H-T_C
ρ_o = density of the fluid
σ = electrical conductivity
μ = fluid viscosity
ν = kinematic viscosity of the fluid
θ = dimensionless temperature, $(T\text{-}T_C)/(T_H\text{-}T_C)$
τ = shear stress in the channel

Subscripts

b = bulk values
C = cold
H = hot

1. Introduction

Laminar natural convection flow in closed loops has been studied by many investigators since it has a considerable number of practical applications in the design of thermal energy systems, thermosyphonic, solar applications and nuclear technologies. When a transverse magnetic field is applied to an electrically conducting fluid in the loop, convective hydrodynamic motion is damped and an electric current is induced.

The method may be very important in control of the thermosyphonic motion in some industrial processes or energy systems that require control of flow

International Journal of Numerical Methods for Heat & Fluid Flow
Vol. 8 No. 7, 1998, pp. 814–840.

The author greatly acknowledges the support of the University Research Board of the American University of Beirut and also the help of Mr Shawki Fattal in performing some of the simulations.

destabilisation or prohibition of motion. Another interest in such a system is novel and appears fairly attractive when a direct energy conversion is envisioned by using the thermosyphonic loop as a magentohydrodynamic electrical generator. In some engineering devices, the MHD situation is brought about as a side effect and may well be utilised for electricity generation. The advantages of such a generator are obvious: it combines in a single unit the functions of a conventional turbine and generator, it has no mechanical moving parts, it can be made perfectly leakproof, and the absence of moving parts makes it possible to use materials permitting operation at very high driving temperature differences. Such an MHD generator can be particularly useful in many specialised engineering applications, e.g. in aircraft.

Several aspects of convective motion characteristics of single-phase closed loop thermosyphon have been much discussed in literature particularly in relation to stability characteristics. Creveling *et al.* (1975) studied the dynamics of the thermosyphonic flow in a single circular loop system exhibiting typical non-linear effects using one-dimensional analysis and they verified their model with experimental observations. Also Erhard *et al.*, (1989) and Davis and Roppo (1987) investigated double-loop thermosyphonic systems, where two circular loops were coupled by a heat exchanger for different coupling locations. Their experiments and mathematical models confirmed the existence of a subcritical buoyancy parameter range for which the flow alternatively exhibited steady state as well as time dependent behaviour.

Recently, Ghaddar (1997) predicted the induced electric current in buoyancy-driven side-heated loop containing an electrically conducting fluid in a transverse magnetic field using an analytical one-dimensional model. Ghaddar's model was based on the use of Hartmann Plane-Poiseuille flow solution for estimating loop shear stress and the 1-D model presented a closed form solution of the steady induced flow and current from which optimal conditions for maximum induced current were derived at low Prandtl number fluids.

No other work has been reported on the effect of a transverse magnetic field for motion control in such loops. Actually other related work reported in the literature has concentrated on buoyancy driven convection in enclosures with the use of a transverse magnetic field to damp hydrodynamic motion, particularly during manufacturing of crystals (Hart, 1983; Vasseur *et al.*, 1995; and Vives and Perry, 1987). Garandet *et al.* (1992) proposed an analytical solution to the equations of magnetohydrodynamics that can be used for the core flow in 2-D shallow cavities (Horizontal Bridgman configuration). Alchaar *et al.* (1995) verified their model and solved the same equations numerically for a wide range of Grashof, Hartmann and Prandtl numbers.

In this work, a numerical two-dimensional solution based on the loop convection in the presence of a transverse magnetic field is developed using the spectral element method. The numerical technique has previously undergone rigorous numerical tests and optimisation for memory and CPU, but modified in this work for the effect of the Lorentz force (Ghaddar 1996; Ghaddar *et al.*,

1986c; Korzsak and Patera, 1986). The two-dimensional model will help us gain insight into the relative influence of the physical parameters involved in the problem and compare the numerical results obtained with the closed-form solution using the Hatmann-Poiseuille model of Ghaddar (1997). The interplay of driving density differences and damping effect of the magnetic forces onto the flow is discussed. The induced electric current is evaluated with the intention to optimise the mechanical/electrical energy conversion.

2. Problem statement

The essential features of the thermosyphonic-closed loop are shown in Figure 1. The loop has a height 2L, an internal channel width of D = 2d. The upper and lower connecting portions of the vertical channel are circular arcs. The fluid contained in the loop is electrically conducting with an electrical conductivity σ, a coefficient of thermal expansion β and a thermal diffusion coefficient α. The magnetic field B_0 is applied perpendicular to the gravity in the x-direction. The thermophysical properties of the fluid at a reference temperature T_0 are assumed to be constant except for the density, which is related to temperature according to the Boussinesq approximation of linear density, variation with temperature, $\rho=\rho_0[1-\beta(T-T_0)]$. The right side of the loop walls is isothermally heated to T_H and the left side of the loop walls is isothermally cooled to T_C, which is taken as the reference temperature T_0. The connecting regions of the loop of projected height *l* on each side are insulated.

3. Mathematical formulation

Neglecting the effect of Joulean heating and viscous dissipation on heat transfer and assuming that the induced magnetic field is very small compared to B_0, the governing two-dimensional equations for continuity, momentum, energy and electric charge are solved in the physical domain shown in Figure 1. The equations are given in non-dimensional form as:

Continuity:
$$\nabla.\vec{V} = 0 \tag{1}$$

Momentum in x-direction:

$$\frac{\partial U}{\partial t} = -(\vec{V}.\nabla)U - \frac{\partial p}{\partial x} + \mathrm{Pr}\,\nabla^2 U \tag{2a}$$

Momentum in y-direction:

$$\frac{\partial V}{\partial t} = -(\vec{V}.\nabla)V - \frac{\partial p}{\partial y} + \mathrm{Pr}\,\nabla^2 V - Ha^2\,\mathrm{Pr}\,V - Gr\,\mathrm{Pr}^2\,\theta \tag{2b}$$

Energy:

$$\frac{\partial V}{\partial t} = -(\vec{V}.\nabla)V - \frac{\partial p}{\partial y} + \mathrm{Pr}\,\nabla^2 V - Ha^2\,\mathrm{Pr}\,V - Gr\,\mathrm{Pr}^2\,\theta \tag{3}$$

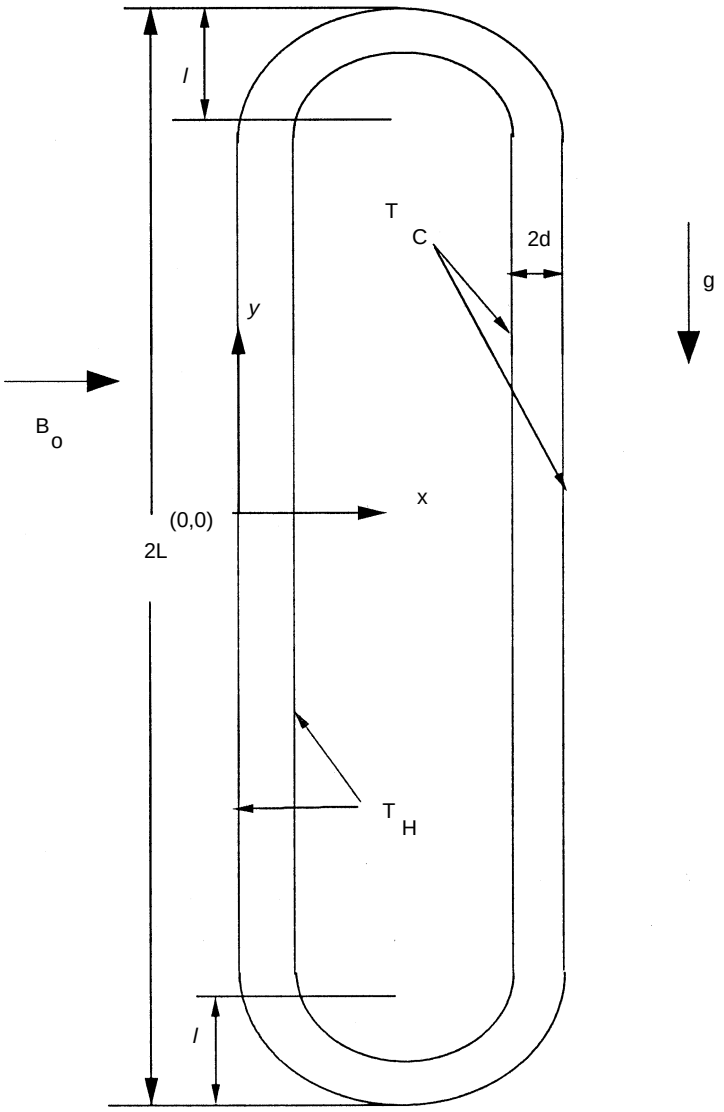

Figure 1.
The essential features of the thermosyphonic closed loop

The electric charge transfer for zero applied electric field gives the induced electric current j in the direction perpendicular to the plane of the magnetic field and flow velocity as:

$$j = \frac{\alpha\sqrt{\mu\sigma}}{D^2}[(U\hat{x}+V\hat{y})\times Ha\hat{x})] \tag{4}$$

The equations (1) to (3) have been reduced to dimensionless form using the following scales: length: D, velocity: α/D, time: D^2/α and temperature: $\theta = (T-$

$T_C)/\Delta T$ where $\Delta T = (T_H - T_C)$. The flow parameters as they appear in the equations are Grashof number, $Gr = g\beta\Delta TD^3/\nu^2$, Ha is the Hartmann number, $Ha = B_0D(\sigma/\rho_0\,\nu)^{1/2}$, and Pr is the Prandtl number, $Pr = \nu/\alpha$. The square of the Hartmann number represents the ratio of the Lorentz force to the viscous forces. (For comparison, the quantity $(\sigma/\rho_0\,\nu)^{1/2}$ for mercury ($Pr \approx 0.02$) is about 2.7×10^5 while for sea water ($Pr \approx 7$) it is about 65.)

The associated boundary conditions of equations (1) to (3) are given by:

$U = V = 0$ on all solid boundaries (5)

$\theta = 1$ $y < |L-l|/D$ and $x < 2.5$ on the left-side wall (6a)

$\theta = 0$ $y > |L-l|/D$ and $x > 2.5$ on the right-side wall (6b)

$$\frac{\partial \theta}{\partial x} = 0 \qquad (L-l)/2d < y < -(L-l)/2d \text{ on solid walls.} \quad (6c)$$

The coupled equations (1)-(3) with boundary conditions (5)-(6) complete the formulation of the problem.

4. Numerical approach

The above coupled system of equations (1)-(3) is solved numerically for the laminar steady-state solution using the spectral element method with the appropriate boundary conditions (Korzsak and Patera, 1986). The numerical approach of the spectral element method is that of direct simulation using initial value solvers. The method is a high order, weighted residual technique that exploits both the common features and the competitive advantages of low-order finite element methods (generality and geometric flexibility) and the p-type spectral techniques (accuracy and rapid convergence).

The temporal discretization of the governing equations is performed using the three-step splitting scheme (Karniadakis *et al.*, 1991). The convective terms and the buoyancy term are incorporated into the non-linear advection explicit integration step using a third order Adams-Bashforth scheme. In the splitting scheme, the applied Lorentz force and the buoyancy force are also incorporated in the non-linear advection term in the explicit integration step. This is followed by a split pressure step that uncouples continuity and pressure equations by using an inviscid pressure boundary condition. The diffusion terms are treated implicitly in a final step using second order Crank-Nicolson schemes. The method has temporal accuracy of order Δt^2 for the velocities and a splitting error of $\Delta t/Re$ for the pressure.

The spatial discretization of the computational domain is done by dividing the domain into general quadrangular macro-elements. Within each element, the dependent and independent variables are presented in terms of high order, tensor-product polynomial expansions with Chebyshev collocation points. Typical grid systems are shown in Figure 2 having 18, 36 and 26 macro elements respectively, with $N \times N$ ($N = 9$) local spectral resolution. Mixed variational and collocation operators are used to generate the discrete equations with interfacial continuity constraints imposed naturally via the variational

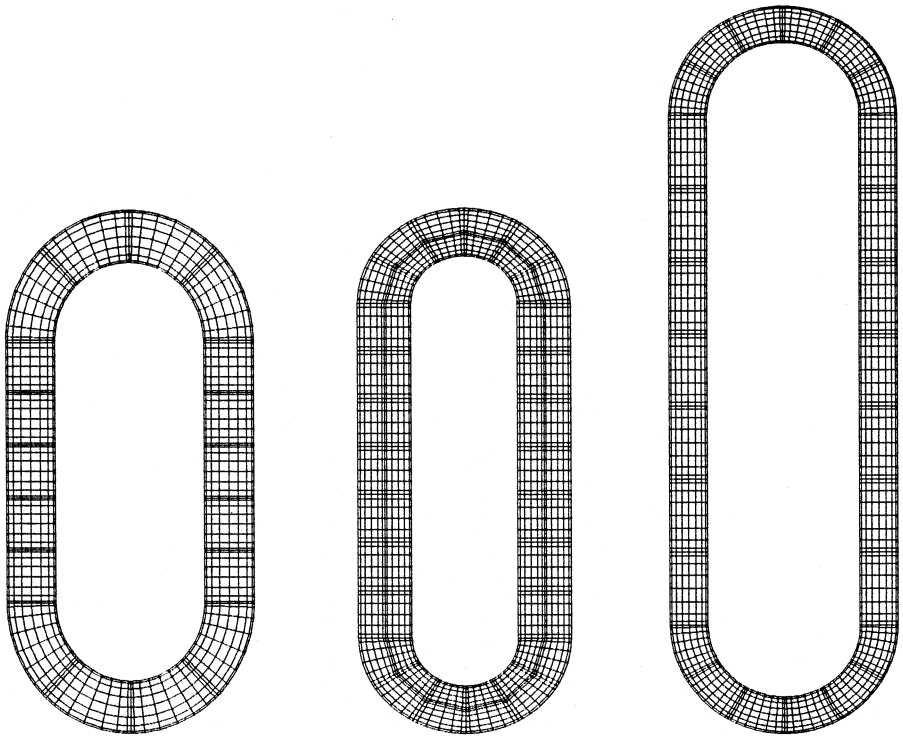

(a) L/d = 10 **(b)** L/d = 10 **(c)** L/d = 20

Figure 2.
Typical grid systems having 18, 36 and 26 macro elements, respectively, with N × N (N = 7) local spectral resolution

statements. The spectral element code had been used and tested for accurately simulating highly unsteady two-dimensional laminar flows with heat transfer (Amon and Guzman, 1996; Ghaddar, 1996; Nigen and Amon, 1993a). Therefore the technique is well suited for our problem.

The computations were performed in double precision on a 586DX2-133MHz PC using the Watcom Fortran Compiler. The time step size Δt for the numerical solution is governed by the Courant number stability condition of $(\Delta t V_{max}/\Delta s) < 0.7$, where Δs is the minimum grid size in either x or y direction. The solutions were checked for convergence in both time-step and spatial degrees of freedom. The convergence criterion was set relative to the change in temperature. Convergence was achieved when the maximum change in temperature was less than 10^{-5}. Figure 3 shows a typical history plot of velocity and temperature for a given point in the domain at (x = 0.5, y = 2) at $Gr = 10^4$, Pr = 1 and Ha =1 where the steady state solution is approached through the solution of the transient equations. An energy balance was performed for each converged simulation to verify that the total heat transferred through the loop isothermal cold walls in the upper half was actually equal to the total heat transferred

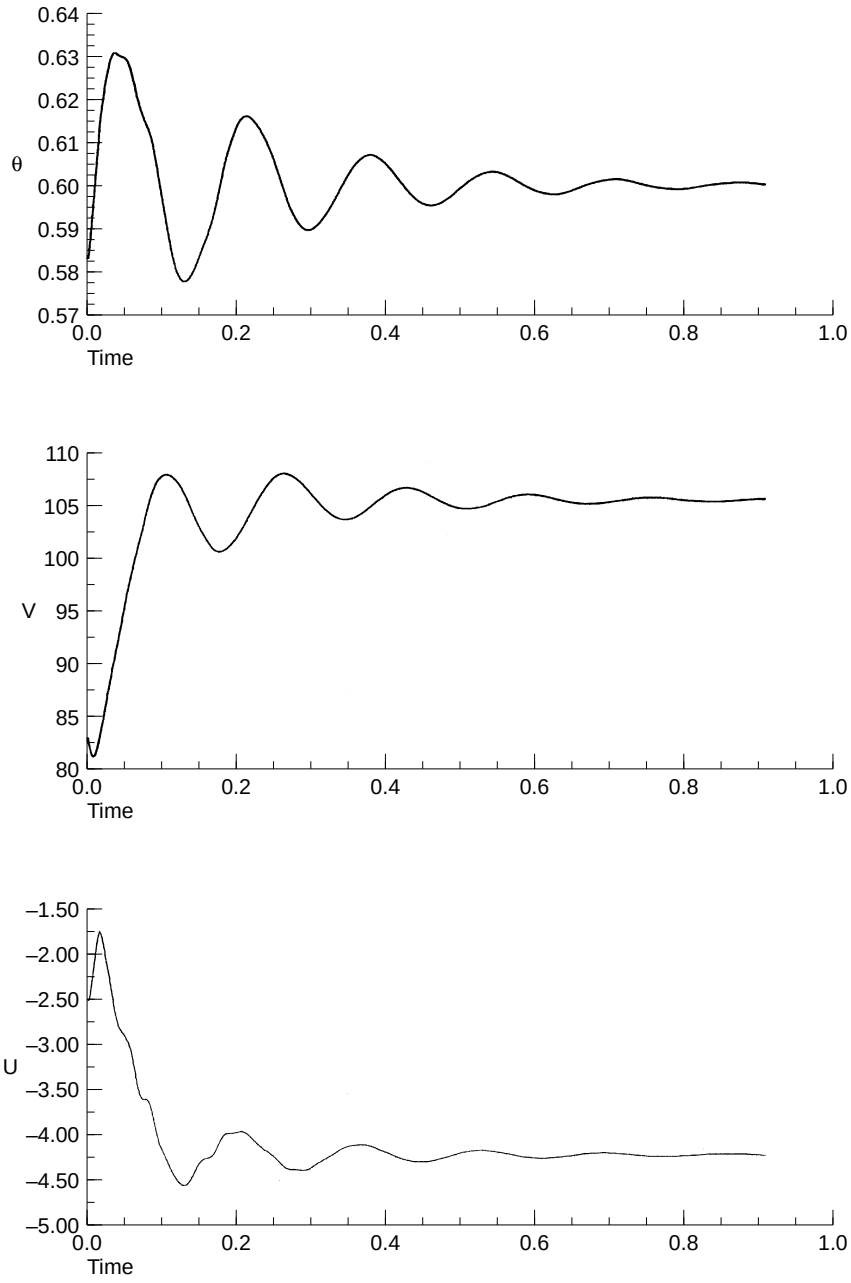

Figure 3.
Typical history plot of velocity and temperature for a point in the domain at (x = 2.5, y = 2) at Gr = 10^5, Pr = 1 and Ha = 5

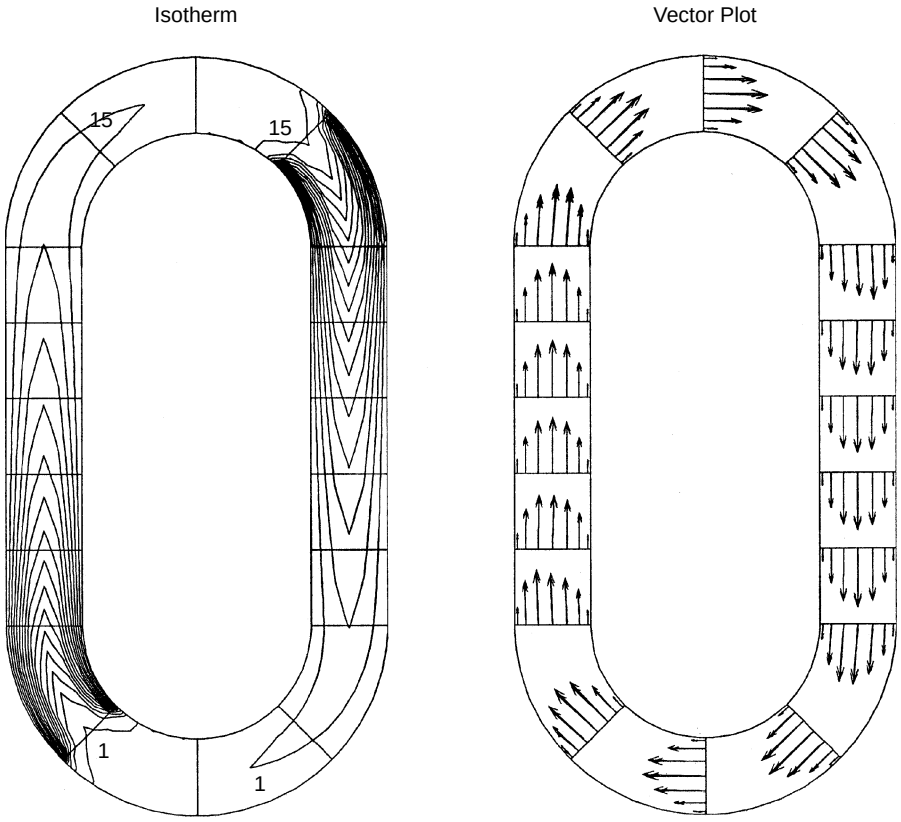

Figure 4a. The isotherms and velocity vector plots of the steady loop flow illustrated for the case of L/d = 10, *l*/L = 0.1, Pr = 1 at Gr = 2×10^3 and Ha = 0

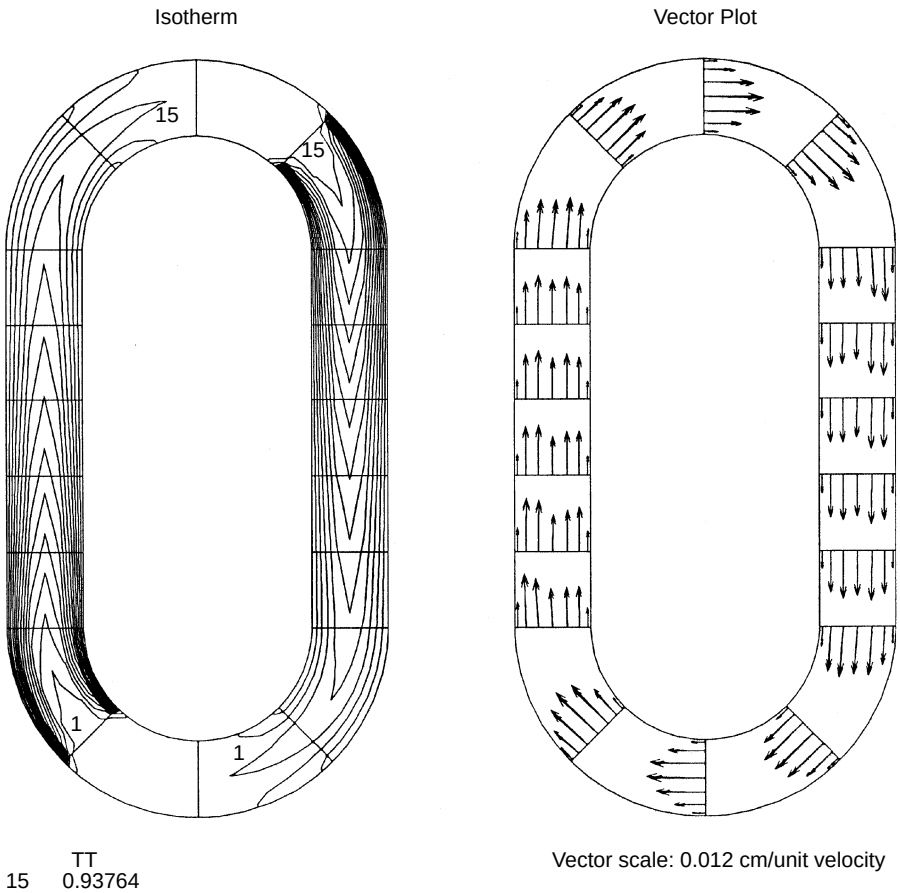

Figure 4b.
The isotherms and velocity vector plots of the steady loop flow illustrated for the case of L/d = 10, *l*/L = 0.1, Pr = 1 at Gr = 10^4 and Ha = 0

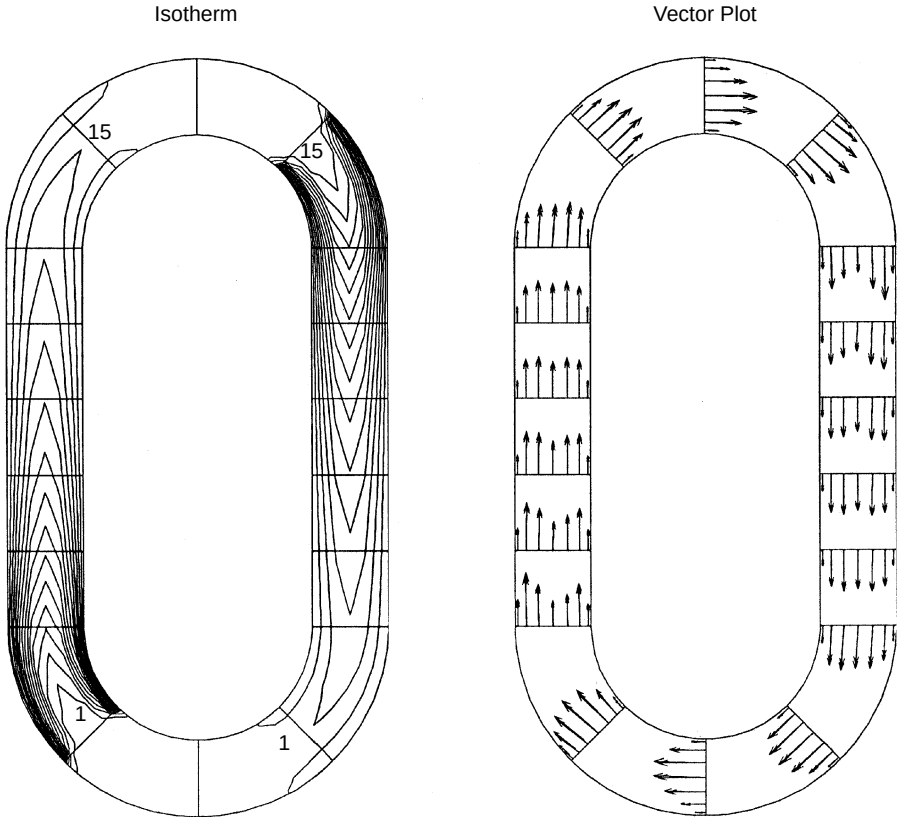

	TT
15	0.93764
14	0.875119
13	0.812599
12	0.750079
11	0.687558
10	0.625038
9	0.562518
8	0.499997
7	0.437477
6	0.374957
5	0.312436
4	0.249916
3	0.187396
2	0.124875
1	0.0623549

$Gr = 1 \times 10^4$, $Ha = 5$

Figure 4c.
The isotherms and velocity vector plots of the steady loop flow illustrated for the case of $L/d = 10$, $l/L = 0.1$, $Pr = 1$ at $Gr = 10^4$ and $Ha = 5$

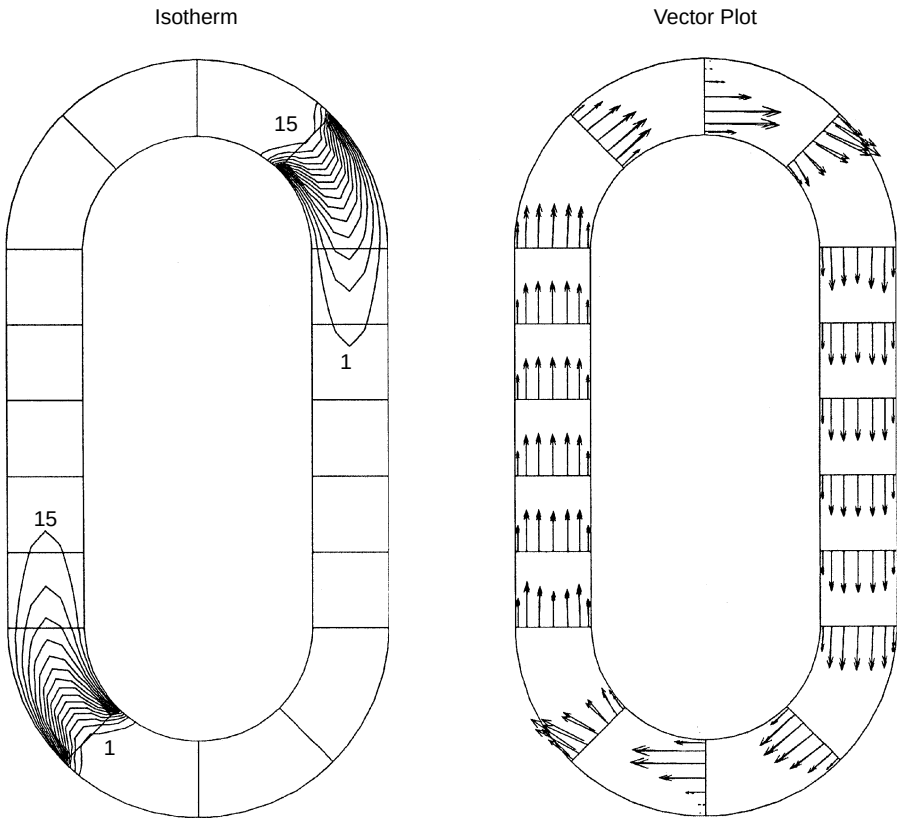

Figure 4d.
The isotherms and velocity vector plots of the steady loop flow illustrated for the case of L/d = 10, *l*/L = 0.1, Pr = 1 at Gr = 10^4 and Ha = 20

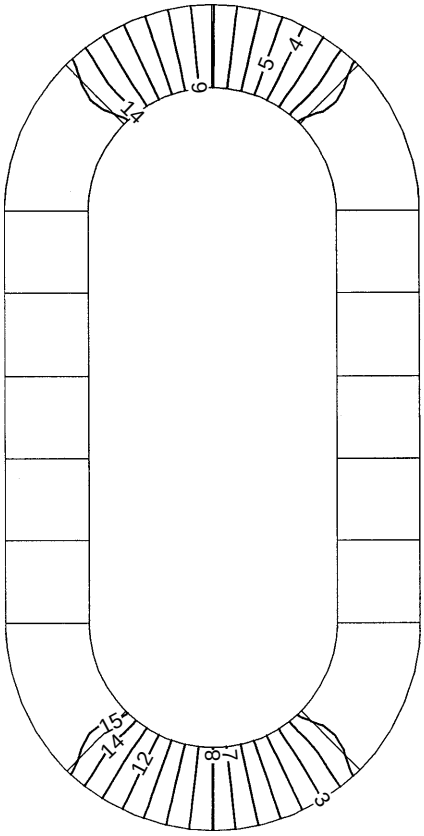

Pure Conduction Case

Level	TT
15	0.93764
14	0.875119
13	0.812599
12	0.750079
11	0.687558
10	0.625038
9	0.562518
8	0.499997
7	0.437477
6	0.374957
5	0.312436
4	0.249916
3	0.187396
2	0.124875
1	0.0623549

Figure 5a.
The isothermal contours of the pure conduction case in the loop

through the hot lower half. At the steady state conditions the error difference in the balance was less than 0.011 per cent.

5. Results and discussions

Electroconducting fluids generally have small Prandtl numbers and consequently inertia effects are expected to be significant even with a small driving temperature difference. In this section, some representative simulation results are presented to illustrate the effect of various controlling parameters on the flow and its thermal behaviour. Computations are also carried out for selected sample runs to compare with the analytical model of Ghaddar (1996).

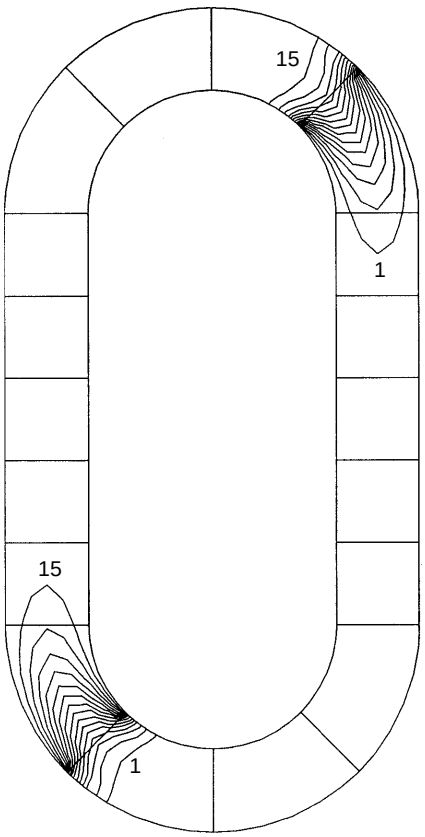

	TT
15	0.93764
14	0.875119
13	0.812599
12	0.750079
11	0.687558
10	0.625038
9	0.562518
8	0.499997
7	0.437477
6	0.374957
5	0.312436
4	0.249916
3	0.187396
2	0.124875
1	0.0623549

Gr = 10^4, Ha = 0, Pr = 0.02

Figure 5b.
The isothermal contours of Gr = 10^4 at Pr = 0.02

5.1 Flow and thermal behaviour of the 2-D side-heated loop

The isotherms and velocity vector plots of the steady loop flow are illustrated in Figures 4(a-d) for the case of L/d = 10, *l*/L = 0.1, Pr = 1 at (a) Gr = 2×10^3 and Ha = 0 (b) Gr = 10^4 and Ha = 0, (c) Gr = 10^4 and Ha = 5 and (d) Gr = 10^4 and Ha = 20. As the Grashof number is increased, the bulk temperature and wall temperature difference increases and the warm and/or cold fluid becomes sharper as it enters the upper and/or lower bends of the loop. The retarding effects of the magnetic drag on the flow pattern is seen Figure 4(c) and 4(d) where the increase in Hartmann number inhibits any convective circulation at the bends' entrances and a more parallel flow is attained. The fluid in the upward going side assumes the wall temperature at almost 1/3 height for the case of Ha = 20 compared to full height at Ha = 5 (compare isotherms of 4(c) and

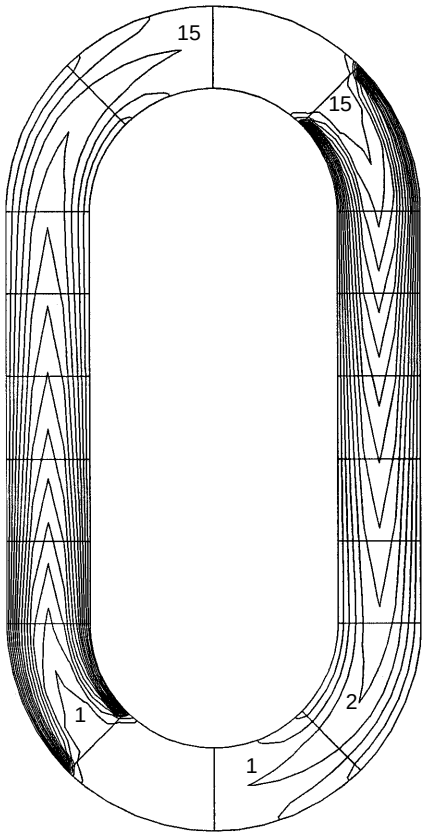

	TT
15	0.93764
14	0.875119
13	0.812599
12	0.750079
11	0.687558
10	0.625038
9	0.562518
8	0.499997
7	0.437477
6	0.374957
5	0.312436
4	0.249916
3	0.187396
2	0.124875
1	0.0623549

Gr = 10^4, Ha = 0, Pr = 1

Figure 5c. The isothermal contours of Gr = 10^4 at Pr =1

4(d)). This is due to decreased convective motions. In all the graphs, the flow in the vertical part of the channel is parallel. Figure 5 shows the isothermal contours of (a) the pure conduction case in the loop, (b) Gr = 10^4 at Pr = 0.02 and Ha = 0 and (c) Gr = 10^4 at Pr=1 and Ha = 0. The isothermal patterns are strongly affected by Prandtl number. At low Prandtl, the weak coupling between momentum and energy equations results in smaller gradients of the isotherms in the domain.

The geometric parameter, L/d, representing the loop height over width, may affect the parallelism of the flow in the channel. Figure 6 shows the velocity vector plots and the isotherms for the cases of Pr = 0.02, Ha = 0, Gr = 10^4 at (a)

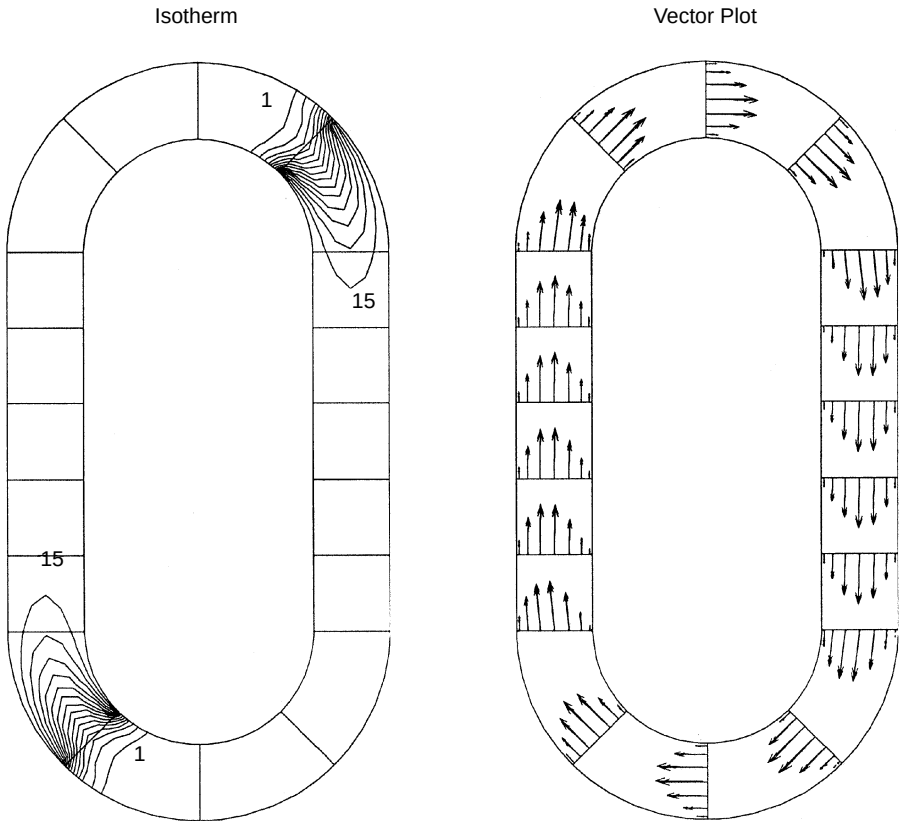

Figure 6a.
The velocity vector plots and the isotherms for the cases of Pr = 0.02, Ha = 0, Gr = 10^4 at L/d = 10 and *l*/L = 0.1

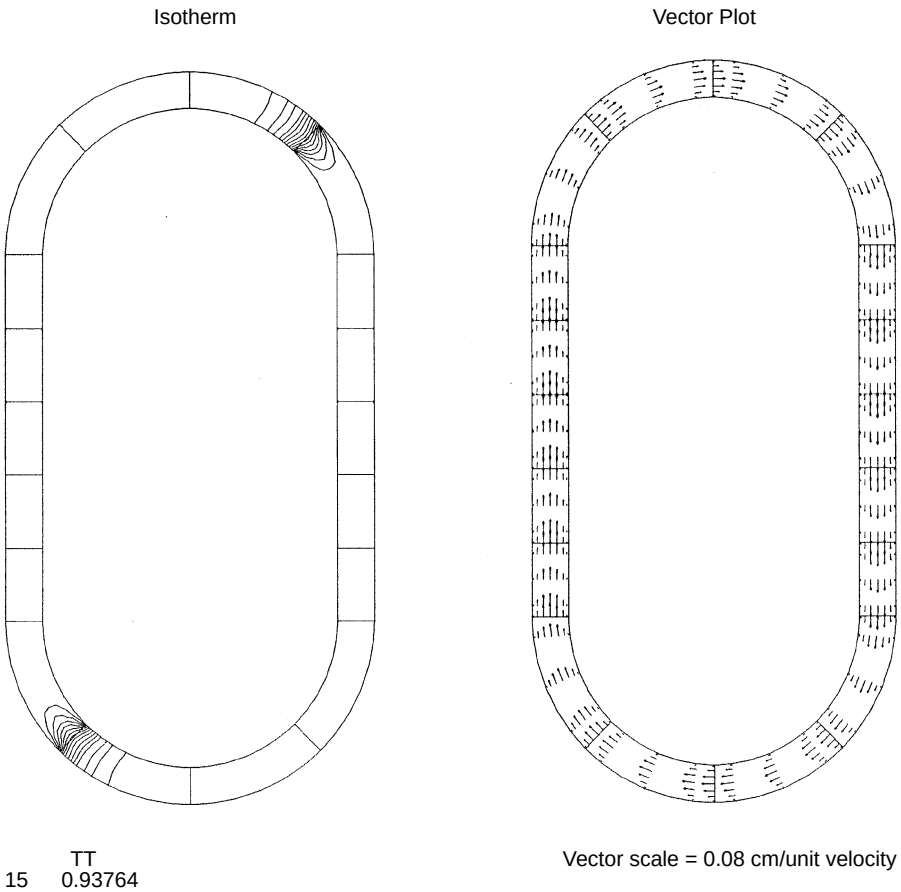

Figure 6b.
The velocity vector plots and the isotherms for the cases of Pr = 0.02, Ha = 0, Gr = 10^4 at L/d = 20 & *l*/L = 0.1

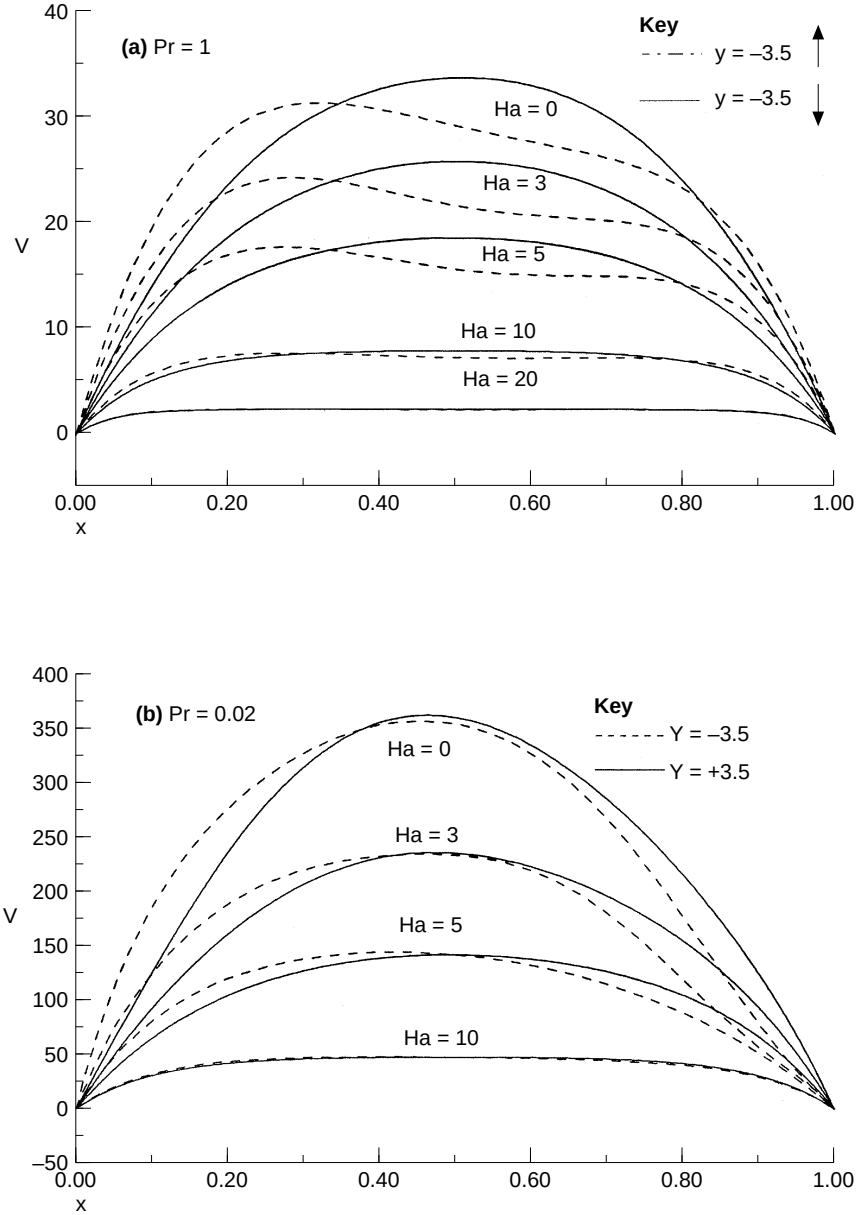

Figure 7.
The velocity profile, V across the channel at y = –3.5 in both the down going flow side and upward going flow, for Gr = 10^4 at various values of Hartmann number, Ha = 0, 5, 10 and 20 for (a) Pr = 1 and (b) Pr = 0.02

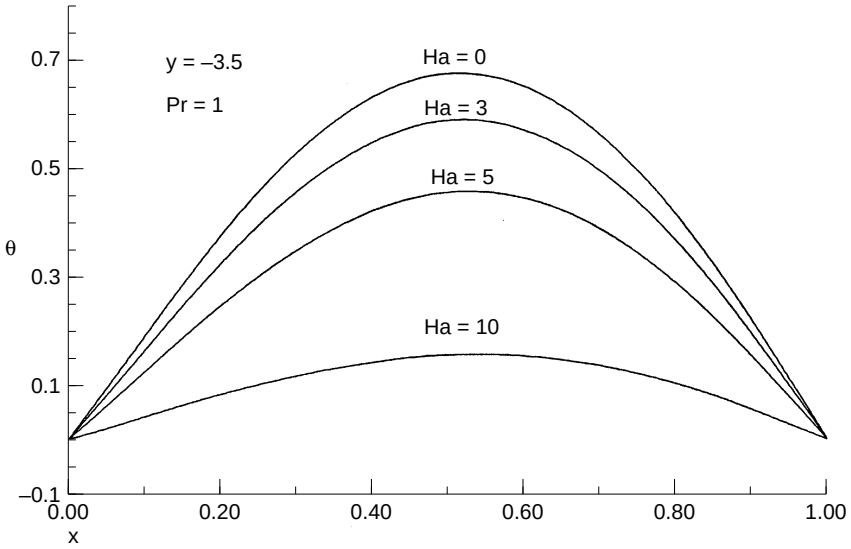

(a)

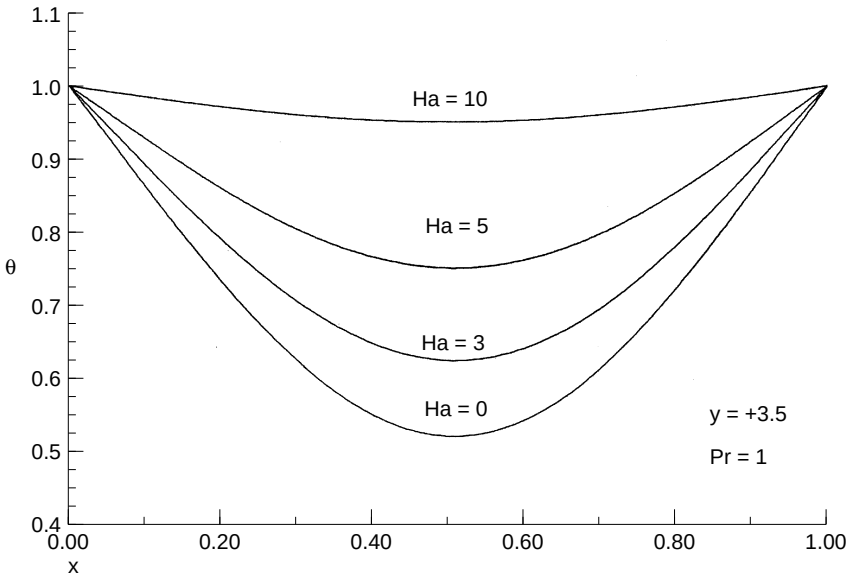

(b)

Figure 8. The dimensionless temperature profiles are shown for the case of a loop with L/d = 10 and *l*/L = 0.1 at (a) y = –3.5 of the upward going flow and for (b) y = +3.5 of the downward going flow for Gr = 2×10^3 at various values of Hartmann number, Ha = 0, 2, 4 and 5.

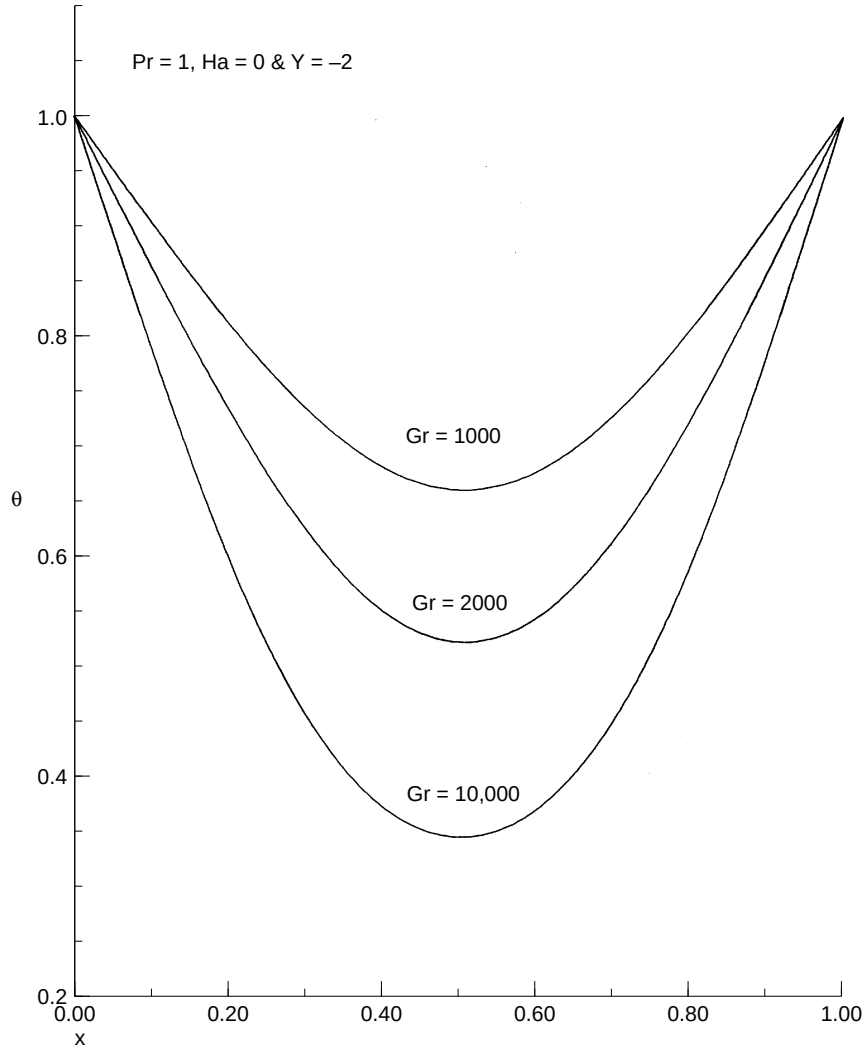

Figure 9.
The temperature profiles at y = –2, Ha = 1, Pr = 1 for different values of Grashof number

L/d = 10 and *l*/L = 0.1 and (b) L/d = 20 and *l*/L = 0.1. It is clear that the parallelism in the flow is disturbed in shorter and thicker channels particularly close to the upper and lower bends.

5.2 Velocity and temperature profiles

Figure 7 shows the velocity profile, V across the channel at y = –3.5 in both the down going flow side and upward going flow for Gr = 10^4 at various values of Hartmann number, Ha = 0, 5, 10 and 20 for (a) Pr = 1 and (b) Pr = 0.02. As the cold fluid is coming through the insulated region into the heated section, the velocity profile becomes sharper due to enhanced motion by buoyancy. The velocity profiles in the cold section, before the fluid enters the insulated section,

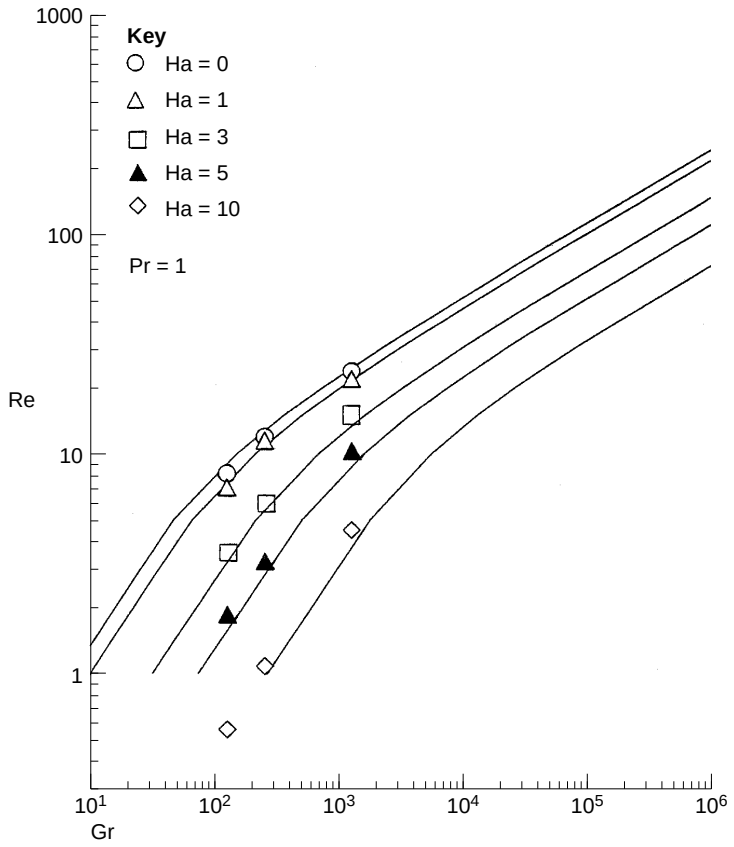

Figure 10. The calculated and analytically predicted Reynolds number of the flow as a function of Grashof number at Ha_d = 0, 3, 5 and 10 for the case of *l*/L = 0.1, L/d = 10 at Pr = 1

have higher velocity gradients than gradients after the fluid enters the hot section. These profiles are similar to plane Poiseuille flow profiles, because by the end of the cold region the fluid bulk temperature has approached the cold wall temperature and the physical situation then resembles a channel flow driven by a pressure gradient. However, the parallelism and symmetry of the flow are maintained for the most part of the channel. For high Hartmann number, the velocity becomes constant over almost the entire section and the shear stress rises at the wall.

In Figure 8, the dimensionless temperature profiles are shown for the case of a loop with L/d =10 and *l*/L = 0.1 at (a) y = –3.5 of the upward going flow and for (b) y = +3.5 of the downward going flow for Gr = 2×10^3 at various values of Hartmann number, Ha = 0, 2, 4 and 5. As Hartmann number is increased, the profiles become flatter and the bulk temperature becomes lower. The difference in the symmetrical parallel profiles at y = ±3.5 is noted due to the fact that one is for a hot fluid entering a cold channel and the other for a cold fluid entering a hot channel in the loop. Figure 9 shows the temperature profiles in the upward moving flow at y = –2, Ha=1, Pr =1 for different values of Grashof number. The

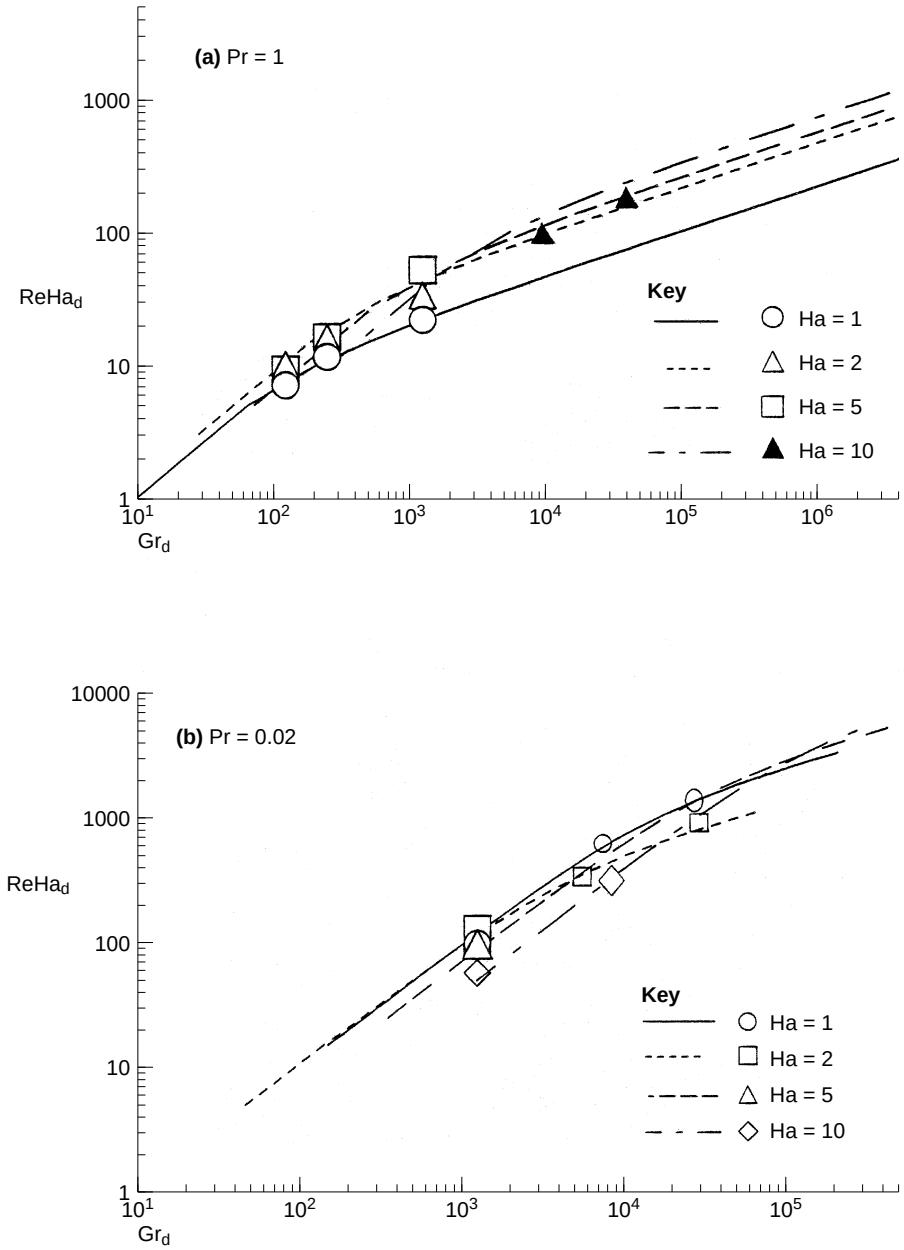

Figure 11.
The calculated and analytically derived electric current expressed in terms of the dimensionless current parameter ReHa = $jd^2/\{\nu(\sigma\mu)^{1/2}\}$, as a function of Grashof number for (a) Pr = 1 and (b) Pr = 0.02

temperature difference between bulk and wall temperature increases as Grashof number is increased.

5.3 Effect of magnetic field on induced velocity; comparison with 1-D model

Of interest here is the relation of the induced velocity to the driving buoyancy force and the retarding Lorentz force. The induced bulk velocity circulating in the loop is calculated from the 2-D simulations at various Grashof and Hartmann numbers. As mentioned earlier, the effect of a transverse magnetic field on buoyancy-driven convection in a loop has been studied recently by Ghaddar (1996) based on the parallel flow approximation for L/d >>1 where a Hartmann-Poiseuille channel flow is used for modelling the shear stress. It was demonstrated in the 1-D model that the average induced bulk velocity is correlated to the Grashof number of the flow by:

$$Gr_d = \frac{4\,\mathrm{Re}_d\, Ha_d^{\,2}\left[1 + \dfrac{\tanh Ha_d}{Ha - \tanh Ha_d}\right]}{2(1 - l/L) - \dfrac{4\,\mathrm{Re}_d\,\mathrm{Pr}[F]}{(L/d)Nu_d}} \qquad \text{“Hartmann Poiseuille Model”} \quad (7)$$

Where Re is the Reynolds number, $Re_d = V_o d/\nu$, V_o is the bulk induced 1-D velocity in the loop, Nu is the Nusselt number, $Nu_d = hd/k$, and F is a bounded parameter ($0 \le F \le 1$) that depend also on the flow Reynolds number, Prandtl number and Nusselt number[2]. The non-dimensional bulk velocity of the calculated two-dimensional flow is related to the Reynolds number of the induced 1-D flow by $Re_d = V_b/^2Pr = 0.5Re$ where $V_b = (1/D)\int_0^1 V dx$ and $Re = V_b D/Pr$. The parameter F was found by Ghaddar (1996) to approach unity for very low Prandtl numbers ($F \to 1$ for $Pr << 1$). The correlation of equation (7) is strictly valid for the limit of L/d>>1, and will be now compared with the 2-D simulation results.

Figure 10 shows the calculated and analytically predicted Reynolds number of the flow as a function of Grashof number at Ha_d = 0, 3, 5 and 10 for the case of l/L = 0.1, L/d =10 at Pr =1. The analytical results of equation (7) are continuous lines; numerical results shown as circles are seen to agree well for the large L/d ratio with both the 1-D models which slightly overpredict the induced flow Reynolds number. Figure 11 shows the calculated and analytically derived electric current expressed in terms of the dimensionless current parameter $Re_dHa_d = jd^2/\{\nu(\sigma\mu)^{1/2}\}$, as a function of Grashof number at L/d = 10 at various values of Hartmann number for (a) Pr = 1 and (b) Pr = 0.02. At fixed Hartmann number, the induced current increases as the Grashof number is increased due to increased buoyancy force that directly affects the flow. The two-dimensional simulation predictions agree well with 1-D model results where the data fall within an error of 5-12 per cent.

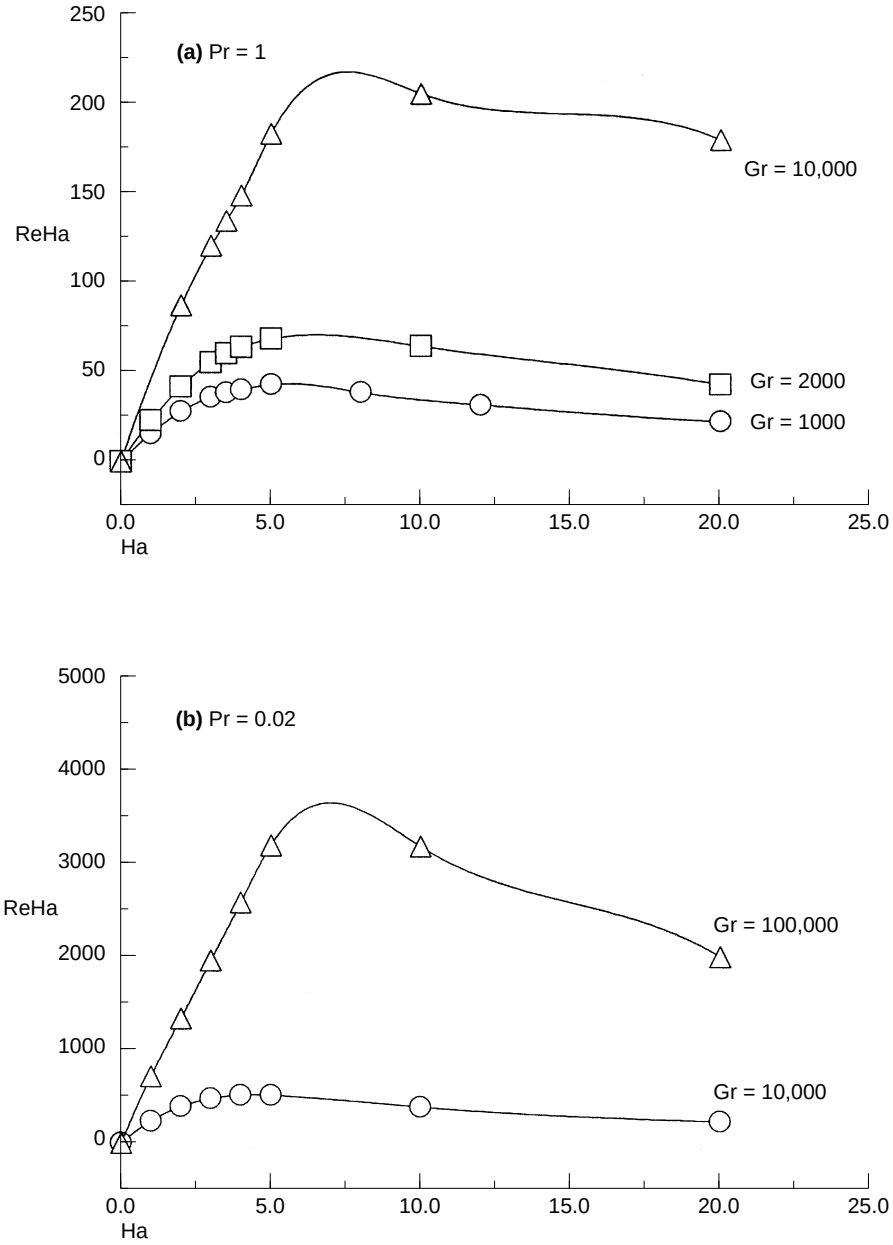

Figure 12.
The 2-D predicted results of the induced electric current as a function of the Hartmann number for (a) Pr = 1 and (b) Pr = 0.02 at different values of Grashof number

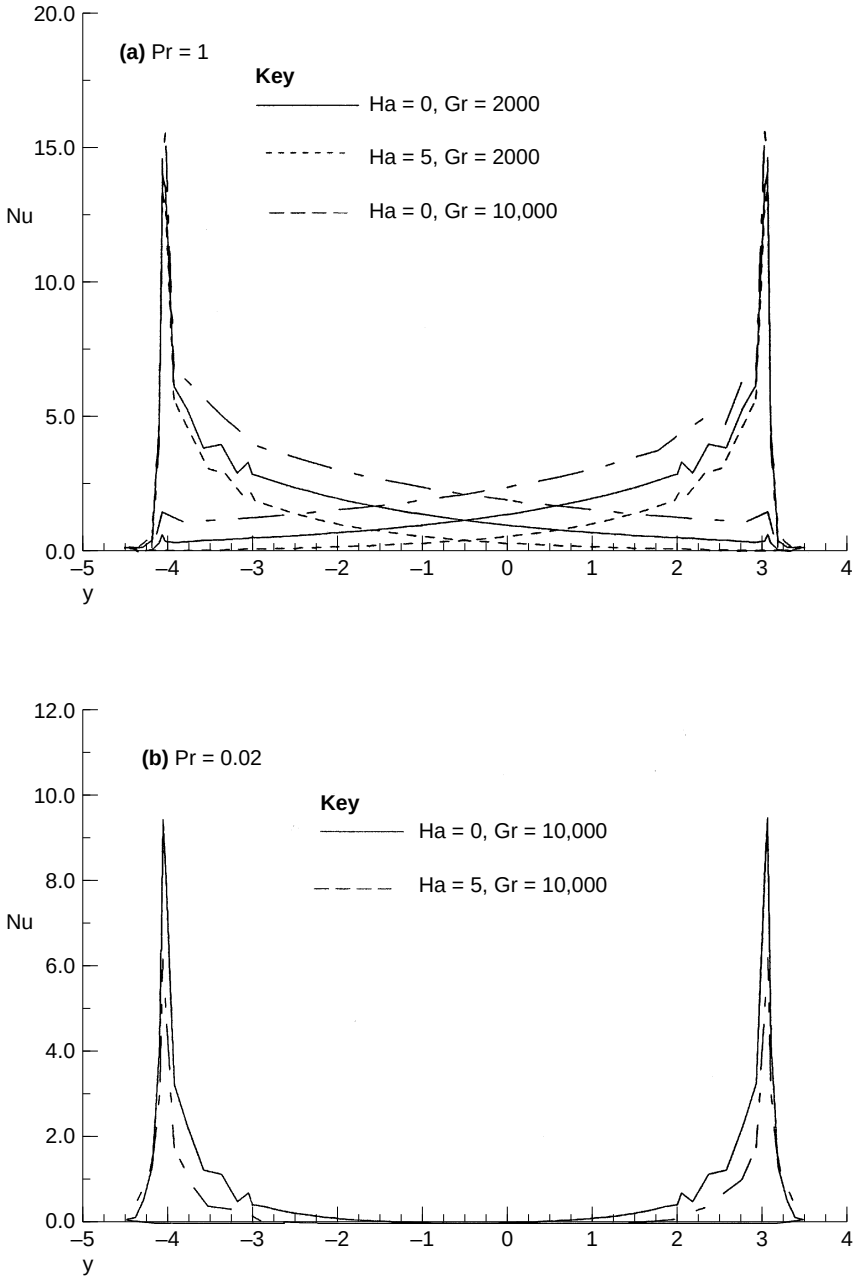

Figure 13. A plot of the heat transfer parameter, Nu is plotted as a function of loop vertical position y, for different values of Hartmann numbers at $Gr = 10^4$, L/d = 10 and *l*/L = 0.1 for (a) Pr = 1 and (b) Pr = 0.02.

5.4 Optimal Hartmann number for maximum induced current

The 1-D model predicted that at low Prandtl numbers, the induced electric current parameter $jd^2/\{\nu(\sigma\mu)^{1/2}\}$had an optimal Hartmann number that maximised the induced current (Ghaddar, 1996). It was interesting that the maximum induced current for low Prandtl fluid occurred at a quite low magnetic field strength and the optimal Hartmann number increased as the Grashof number increased. In the present 2-D model, a number of simulations are performed at fixed Grashof numbers to locate the optimal Hartmann number for Pr = 1 and Pr = 0.02, and complete the comparison with 1-D model.

Figure 12 shows the 2-D predicted results of the induced electric current as a function of the Hartmann number for (a) Pr = 1 and (b) Pr = 0.02 at different values of Grashof number at L/d = 10, based on 2-D computer simulations. It is very clear that a peak of J existed at an optimal value of Hartmann number, Ha_{opt}, not only for low Prandtl number but also for Pr = 1. This optimal strength of the magnetic field is weakly dependent on Grashof number as predicted by the 1-D models for low Prandtl numbers. For example at for Pr = 0.02, the maximum current is at Ha_{opt} = 4.2, and 7.2 for Gr = 10^4 and 10^5 respectively. For Pr =1 Ha_{opt} = 5.1, 6.2 and 6.8 for Gr = 10^3, 2×10^3 and 10^4 respectively. The optimal Hartmann number increases as Grashof number is increased consistent with 1-D predictions. The 1-D model predicted H_{opt} for low Prandtl number to follow closely the correlation (Ghaddar, 1996):

$$(Ha_{opt})_f = \sqrt{12 + \frac{Gr\,\mathrm{Pr}}{2Nu(L/D)}} \qquad \text{for } \mathrm{Pr}<<1 \tag{8}$$

which gives a higher estimation of about 2-13 per cent than the 2-D model. This is explained by the presence of the circular upper and lower parts of the loop where the curvature adds a higher drag to the flow as compared with the straight channel model. The higher the L/d ratio, the better the representation is of the 2-D simulations with the 1-D analytical model. The 2-D simulation has shown the existence of an optimal Hartmann number for Pr = 1 which is not reported in the 1-D model.

In the laminar range of the induced steady flow, the presence of H_{opt} is very significant in terms of improving the system efficiency of conversion from thermal/mechanical to electrical in the system in presence of a lower strength magnetic field. The heat transfer carried from the heat source (hot left side of the loop) to the heat sink (cold right side of the loop) is given by:

$$\frac{Qd}{k\Delta T} = \left(\frac{\partial\theta}{\partial n}\right) = Nu \tag{9}$$

where Nu represent the local Nusselt number taken along either of the un-insulated isothermal portions. In Figure 13, the heat transfer parameter, Nu, is plotted as a function of loop vertical position y, for different values of Hartmann numbers at Gr = 10^4, L/d = 10, *l*/L = 0.1 for (a) Pr =1 and (b) Pr = 0.02. The

Nusselt number is maximum as the fluid exits the insulated region to either the heated wall or to the cooled wall, and as the fluid bulk temperature approaches the wall temperature, the Nusselt number drops way below the plane Poiseuille fully developed Nusselt number of 3.77. The rate of heat transfer in presence of a magnetic field decreases as Hartmann number is increased, at fixed Grashof number.

Conclusions

A numerical two-dimensional analysis was carried out using the spectral element method to study the hydrodynamics and heat transfer of buoyancy-driven electrically-conducting fluid in a vertical loop placed in a transverse magnetic field. The numerical model results were compared with the closed form analytical one-dimensional solution of Ghaddar (1996). At high Grashof number only a low strength magnetic field is required to get a significant induced electric current.

Future work will address the optimisation of the system parameters to arrive at conditions that maximise the induced electric current and to consider the conversion efficiency of thermal/mechanical to electrical energy of the described magnetohydrodynamic generator.

References

Alchaar, S., Vasseur, P. and Bilgen, E. (1995), "Natural convection heat transfer in a rectangular enclosure with a transverse magnetic field," *ASME Journal of Heat Transfer,* Vol. 117, pp. 668-673.

Amon, C.H., Guzman, A.M. and Merol, B. (1996), "Lagrangian chaos, Eulerian chaos, and mixing enhancement in converging-diverging channel flows", *Physics of Fluids,* Vol. 8 No. 5, pp. 1192-1206.

Creveling, H.F., De Paz, J.F., Baladi, J.Y. and Schoenhals, R.J. (1975), "Stability characteristics of a single-phase free convection loop," *Journal of Fluid Mechanics,* Vol. 67, part 1, pp. 65-84.

Davis, S.H. and Roppo, M.N. (1987), "Coupled Lorenz oscillators", *Physica D,* Vol. 24, pp. 226-42.

Ehrhard, P., Karcher, Ch., and Muller, U. (1989), "Dynamical behaviour of natural convection in a double loop system," *Experimental Heat Transfer*, Vol. 2, pp. 13-26.

Garandet, J.P., Alboussieri, T. and Moreau, T. (1992), "Buoyancy driven convection in a rectangular enclosure with a transverse magnetic field," *Int. J. Heat Mass Transfer,* Vol 35 No. 4, pp. 741-8.

Ghaddar, N.K. (1996), "Natural convection over rotating cylindrical heat source in an enclosure", *AIAA J.Thermophysics and Heat Transfer,* Vol. 10 No. 2, pp. 303-12.

Ghaddar, N. (1997), "Analytical model of a side-heated free convection loop placed in a transverse magnetic field", *ASME Fluid Engineering Journal,* in press.

Ghaddar, N.K., Karniadakis G.E. and Patera A.T. (1986), "A conservative isoparametric spectral element method for forced convection: application to fully-developed flow in periodic geometries", *Numerical Heat Transfer*, Vol. 9, pp. 227-300.

Hart, J.E. (1983), "Low Prandtl number convection between differentially heated end walls", *Int. J. Heat Mass Transfer*, Vol 26, pp. 1069-74.

Karniadakis, G.E., Isreali, M. and Orszag, S.A. (1991), "High-order splitting methods for the incompressible Navier-Stokes equations", *Journal of Computational Physics*, Vol. 97, pp. 414.

Korzsak, K.Z. and Patera, A.T. (1986), "An isoparametric spectral element method for solution of the Navier-Stokes equations in complex geometries", *J. Computational Physics,* Vol. 62, pp. 361-79.

Nigen, J. and Amon, C.H. (1993), "Forced convective cooling enhancement of electronic package configurations through self-sustained oscillatory flows," *ASME J. of Electronic Packaging*, Vol. 115, pp. 356-65.

Vasseur, P., Hasnaoui, M., Belgen, E. and Robillard, L. (1995), "Natural convection in an inclined fluid layer with a transverse magnetic field: analogy with a porous medium", *ASME Journal of Heat Transfer,* Vol. 117, pp. 121-9.

Vives, C. and Perry, C. (1987), "Effects of magnetically damped convection during the controlled solidification of metals and alloys", *Int. J. Heat Mass Transfer*, Vol. 30, pp. 479-96.